

## The quantitative relationship between non-linear stress-strain behaviour and dislocation structure in martensitic stainless steel

Chamakura, J. N.; Riemslag, A. C.; Reinton, T. E.; Popovich, V. A.; Sietsma, J.

**DOI**

[10.1016/j.actamat.2022.118364](https://doi.org/10.1016/j.actamat.2022.118364)

**Publication date**

2022

**Document Version**

Final published version

**Published in**

Acta Materialia

**Citation (APA)**

Chamakura, J. N., Riemslag, A. C., Reinton, T. E., Popovich, V. A., & Sietsma, J. (2022). The quantitative relationship between non-linear stress-strain behaviour and dislocation structure in martensitic stainless steel. *Acta Materialia*, 240, Article 118364. <https://doi.org/10.1016/j.actamat.2022.118364>

**Important note**

To cite this publication, please use the final published version (if applicable). Please check the document version above.

**Copyright**

Other than for strictly personal use, it is not permitted to download, forward or distribute the text or part of it, without the consent of the author(s) and/or copyright holder(s), unless the work is under an open content license such as Creative Commons.

**Takedown policy**

Please contact us and provide details if you believe this document breaches copyrights. We will remove access to the work immediately and investigate your claim.



# The quantitative relationship between non-linear stress-strain behaviour and dislocation structure in martensitic stainless steel



J.N. Chamakura\*, A.C. Riemslag, T.E. Reinton, V.A. Popovich, J. Sietsma

Department of Materials Science and Engineering, Delft University of Technology, Mekelweg 2, Delft, CD 2628, the Netherlands

## ARTICLE INFO

### Article history:

Received 6 March 2022

Revised 28 August 2022

Accepted 13 September 2022

Available online 15 September 2022

### Keywords:

Anelastic behaviour

Dislocation structure

Cyclic micro-plasticity

Cyclic stress-strain curve

Stainless steel

## ABSTRACT

The reversible behaviour of metals at low applied stresses is more complex than the generally assumed linear behaviour. This is primarily because of the reversible nature of dislocation motion leading to a strain contribution known as anelasticity. This work aims to investigate (a) quantification of dislocation structures in industrial grade stainless steels, (b) unloading behaviour, and (c) the fundamentals of reversible and mechanical behaviour occurring below the yield stress. Mechanical testing of martensitic stainless steel (Stavax ESR) was performed in two different modes: incremental plastic deformation and cyclic loading-unloading below the yield stress with a focus on the measurement of small strains and corresponding stresses, occurring in the pre-yield regime. The non-linear reversible behaviour was quantitatively analysed, as opposed to the common approximation of an empirical determination of apparent Young's modulus. The recently proposed pre-yield model has been refined and, for the first time, successfully applied to a complex microstructure such as stainless steel. The quantification of dislocation structure parameters is shown to be an efficient alternative to the conventional experimental methods of quantifying dislocation structure. Further, a unique representation and quantification of the unloading and hysteresis behaviour provides more insight into the material behaviour. Lastly, the little studied microplasticity occurring below the yield stress upon cyclic loading-unloading was determined. Importantly, the physical basis of the model will allow quantification of plastic deformations in the pre-yield region, large enough to be significant in industrial processes.

© 2022 The Authors. Published by Elsevier Ltd on behalf of Acta Materialia Inc. This is an open access article under the CC BY license (<http://creativecommons.org/licenses/by/4.0/>)

## 1. Introduction

Industrial high-tech equipment such as fine positioning stages, lithographic equipment, robotic arms, and surgical tools require high positioning precision ranging from micrometre to sub-nanometre magnitude [1,2]. The loads applied on the material are low and the deformation is in principle reversible. To conform to the precision standards in the design and manufacture of structures for such applications, it is crucial to understand and predict stress-strain behaviour at stresses below the yield stress, i.e., in the pre-yield regime.

Dislocations are defects present in any metal with densities in the range of  $10^{11}$ – $10^{15}$   $m^{-2}$  [3]. Movement of these dislocations within a material enables plastic deformation at higher loads, but also affects the mechanical behaviour at lower loads. It has been seen experimentally that metals show a nonlinear loading behaviour deviating from Hooke's Law in the pre-yield regime [4–6].

This is due to the short-range movement of dislocation segments leading to anelasticity [6–9]. The dislocation segments which are impeded by pinning points bow out, causing a strain component that is additional to the elastic lattice strain. This, in turn, results in the frequently observed reduction of the apparent Young's modulus. In recent literature, this anelastic behaviour was studied in various steels [6–8,10]. However, for martensitic stainless steels, which are widely used in high-tech applications in components involving flexure mechanisms for their high yield strengths, the anelastic behaviour has not been studied before. A detailed study into this anelastic behaviour in this steel is carried out in this work for quantitative analysis of the dislocation structure and to understand its correlation with mechanical behaviour.

Additionally, it has been seen experimentally that metals show a nonlinear stress-strain relationship during unloading as well [10–16]. The unloading behaviour of metals is of importance for spring-back prediction. This behaviour changes after the metal is plastically deformed [4,6,17,18]. This is caused by an extra reversible strain occurring during loading and unloading along with the purely elastic strain [19]. And, this phenomenon is due to short-range reversible movement of the dislocation segments [7,8,20].

\* Corresponding author.

E-mail address: [j.n.chamakura@tudelft.nl](mailto:j.n.chamakura@tudelft.nl) (J.N. Chamakura).

The dislocation segments which are impeded by the pinning points or that are piled up before the grain boundaries, can move to a new equilibrium upon the relaxation of the applied stress, contributing to some extra microscopic strain during unloading.

Usually, dislocation density is measured using X-Ray Diffraction (XRD) or Transmission Electron Microscopy (TEM). However, there are certain drawbacks associated with the use of these methods. The sample preparation for both TEM and XRD plastically deforms the sample, thereby affecting the dislocation structure. TEM analysis requires time-consuming sample preparation, which induces changes in internal stresses due to the limited thickness of the sample, which is less than a few hundred nanometres [21,22]. As a result, the 3D dislocation segment structure is distorted, and dislocation segments may extend from the top to the bottom surface of the sample. Furthermore, there is a risk of dislocations being omitted and/or not detected during the measurement. In XRD, plastic deformation due to sample preparation translates into peak broadening, which affects the dislocation density calculations [23]. In addition, no information on the dislocation segment length is obtained. And, dislocation density measurements using XRD analysis require complex post-processing of data, which affects the precision and accuracy of the measurements [24]. Furthermore, in some steels, such as the martensitic stainless steels studied in this work, internal stresses developed due to shear transformation from austenite to martensite also contribute to peak widths. Therefore, X-ray line profile analysis leads to inaccuracies in dislocation density measurements, and it is not a suitable method for characterizing dislocation density [25].

The research objective of this paper is to investigate the fundamentals of non-linear stress-strain mechanical behaviour below the yield stress in industrial grade stainless steel. We perform mechanical testing in two kinds of cyclic loading modes: with incremental plastic deformation and, at stresses below the yield stress without plastic deformation. The first kind of test allows to analyse the mechanical behaviour based on dislocation structure in steels using quantitative models. The nonlinearity in the slope of the stress-strain curve in the pre-yield region is quantitatively analysed [4,7]. This analysis provides insight into the non-linear unloading behaviour with varying plastic strain. The second kind of test provides insight into the micro-plasticity that occurs even at stresses well below the yield stress upon cyclic loading-unloading.

First, we determine the range of yielding and dislocation structure parameters from extended Kocks-Mecking plots [7]. The dislocation density measurement using the method described in this paper is shown to be an efficient alternative to the conventional XRD and TEM methods of quantifying dislocation structure. Second, we analyse non-linear behaviour during unloading for different degrees of plastic strain and, therefore, different dislocation densities. And last, we represent and quantify microplasticity observed below yield stress upon cyclic loading-unloading. The physical basis of the model is useful for predictive and quantitative modelling of the behaviour on low stress loading of various metals.

## 2. Materials and methods

### 2.1. Materials

The material used for this study is medium carbon martensitic stainless steel (Stavax ESR) with a sheet thickness of 2 mm. The chemical composition of the steel is shown in Table 1. In this experiment to characterise the microstructure of the material, Stavax steel specimens were ground and polished down to 1  $\mu\text{m}$  finish using diamond suspension, ultrasonically cleaned with ethanol at room temperature. Specimens were etched using Villella's reagent (1 g picric acid, 5 mL concentrated HCl, 100 mL ethanol) for 20 s before proceeding to observe the microstructures by optical and

**Table 1**  
Chemical composition (in wt%) of the investigated Stavax stainless steel [26].

C	Mn	Si	Cr	V
0.38	0.5	0.9	13.6	0.3

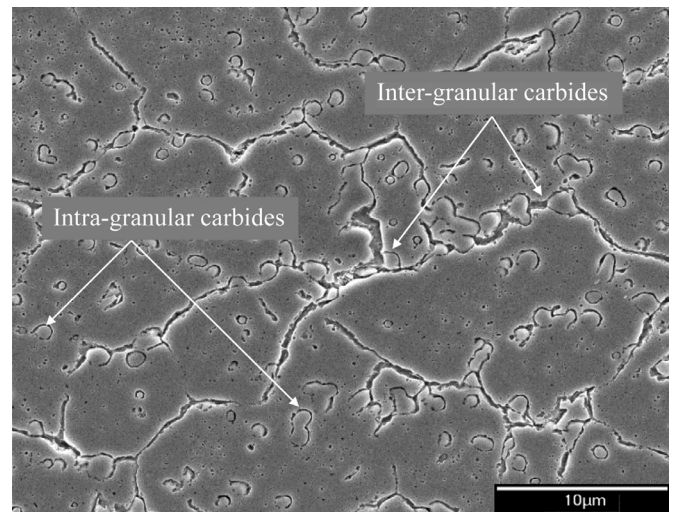


**Fig. 1.** Scanning electron microscope (SEM) micrograph of Stavax steel showing a tempered martensitic matrix with inter- and intra-granular carbides.

scanning electron microscopy. Fig. 1 refers to the microstructure of martensite in Stavax steel. X-ray diffraction was performed to obtain information on microstructural constituents such as carbides and retained austenite. The microstructure of Stavax consists of a tempered martensitic matrix with homogeneously distributed carbides along grain boundaries and within grains, as seen in Fig. 1. The fraction of these carbides, identified to be of the type  $M_{23}C_6$  both from Thermo-Calc software and X-ray diffraction measurements, is around 3% by volume. The microstructure also contains around 5% retained austenite by volume.

### 2.2. Mechanical testing

Tensile testing was carried out using a 25 kN MTS 858 tabletop system equipped with MTS hydraulic collet grips (type 646) and the MTS 609 alignment fixture. The collets grip through friction, which ensures a consistent alignment without introducing plasticity in the gripping section. Before testing, the load train was aligned using a cylindrical strain-gauged specimen in combination with an alignment fixture, resulting in bending strains below 20 microstrain. Elongation was measured by an MTS extensometer (type 632.29F-30) with a 6 mm gauge length and a strain range of  $\pm 4\%$ . Four identical sub-size tensile specimens were machined by electrical discharge machining for each kind of test. This technique was preferred to minimise specimen work hardening, waste, and for its high accuracy. The flat dog bone tensile test specimens illustrated in Fig. 2 (a) were dimensioned with a uniform length of 32 mm, a gauge length of 25 mm, and a width of 10 mm according to the testing requirements of the ASTM E8 standard [27].

In Table 2, the mechanical test plan is provided for the mechanical tests performed. The tensile tests were conducted at a constant strain rate (from the extensometer channel) and at a sampling frequency of 102 Hz. Further, the extensometer was calibrated, and the system tuned for PID values for this steel before testing. In post-yield cyclic testing, the sample is plastically deformed to 0.5% strain and un-loaded and re-loaded to an additional plastic strain of 0.5% for five consecutive cycles at a strain rate of  $1 \times 10^{-4} \text{ s}^{-1}$ . This test serves as the basis for testing the pre-yield model [7] ap-

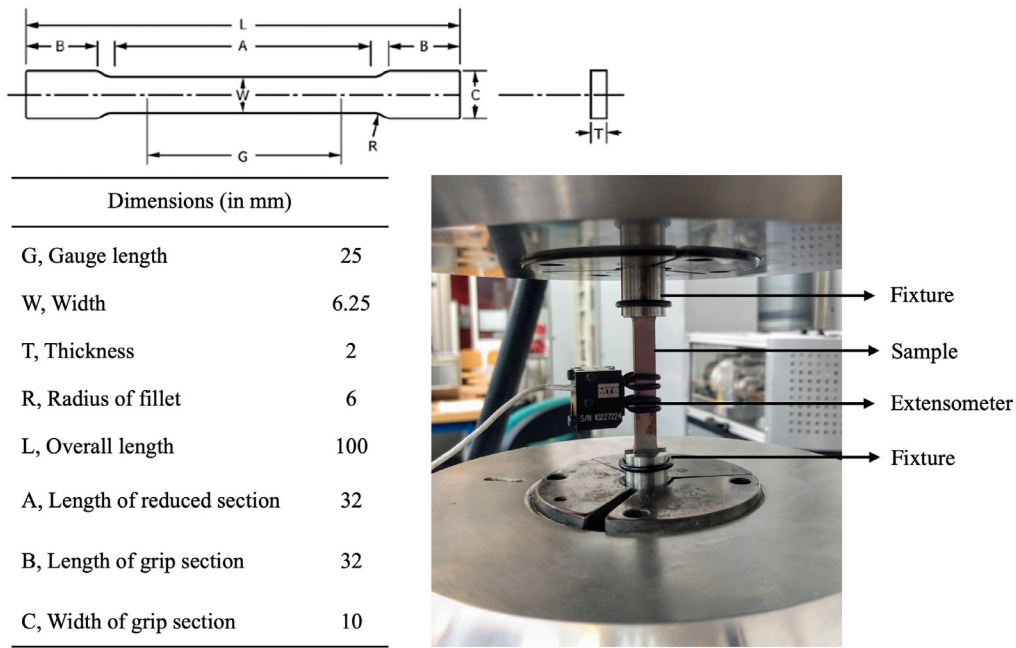


Fig. 2. Schematic of a tensile test specimen (ASTM E8) and sample between grips in MTS 858 tabletop system.

Table 2  
Mechanical test plan.

Test	Method	Control	Strain rate (s <sup>-1</sup> )
Post-yield cyclic testing	Step 1: Pre-load to 8 MPa /100 N Step 2: 5 cycles with 0.5% plastic strain increment in each cycle	Force Strain	1*10 <sup>-4</sup>
Pre-yield cyclic testing	Step 1: Pre-load to 8 MPa /100 N Step 2: 10 cycles below the yield stress at two maximum load levels	Force Strain	2*10 <sup>-5</sup>

plied to the pre-yield range in each loading cycle. In each cycle of plastic deformation, the dislocation structure alters, and the pre-yield model is applied to quantify the dislocation structure in terms of the dislocation density and average segment length, as outlined in Section 3.1. In pre-yield cyclic testing, the sample is loaded to a certain stress level below the yield stress and unloaded to the initial pre-load of 8 MPa for five consecutive cycles. The strain rate is low in the pre-yield cyclic testing (2\*10<sup>-5</sup> s<sup>-1</sup>) to optimise the data acquisition at the same sampling frequency. This test can provide insight into the hysteresis and reversibility of strain behaviour before the onset of plastic deformation.

### 2.3. Theoretical background

Anelasticity, as it is known, has four definitions in literature. One refers to the time-dependent recovery of elastic deformation, and the second describes properties of solids, for which stress and strain are not uniquely related, which makes this behaviour essentially time-independent, given by Zener and Hollomon [19]. A third definition recently proposed in Li and Wagoner describes it as a mode of deformation that is recoverable and energy dissipative [6]. The fourth definition of anelasticity, which we adopt in this paper, refers to the strain caused by the bowing of dislocations, as taking place below the critical stress at which the dislocation segment becomes an activated Frank-Read source.

In the pre-yield regime, the stress-strain curve is usually presumed linearly elastic, following Hooke's law, meaning that the deformation in this regime is reversible and proportional to the applied stress. This linear elastic behaviour is attributed to the stretching of the interatomic bonds in the lattice. The deformation

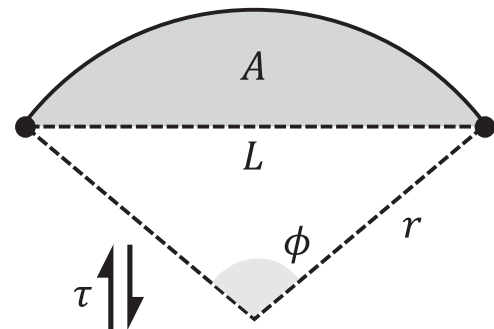


Fig. 3. Dislocation segment with length  $L$  (dashed line) between two pinning points bows out under an applied stress  $\tau$ . The area  $A$  swept by the dislocation segment is proportional to the anelastic shear strain. It is part of a circle with radius  $r$  and subtended angle  $\phi$ .

in the pre-yield regime is in fact of a non-linear nature, since the strain due to bowing out of dislocations also contributes to the deformation. This additional strain is referred to as anelastic deformation in this paper (as seen in Fig. 3). Under increasing stress up to the yield stress, the dislocations bow out to a critical configuration and form loops, i.e., they act as dislocation sources under the Frank-Read mechanism [28]. This leads to an increase in the dislocation density and plastic strain. When a dislocation segment of length  $L$  bows out such that  $r = \frac{1}{2}L$  with  $r$  the radius of curvature, the Frank-Read source reaches its critical state (Fig. 3) and  $r$  reaches a minimum value. Further, if the resolved shear stress is increased above this critical stress, the dislocation segment be-

comes unstable. The critical resolved shear stress ( $\tau_c$ ) of a Frank-Read source is then given by,

$$\tau_c = \frac{Gb}{L} \text{ and } \sigma_c = \frac{MGb}{L} \quad (1)$$

where,  $\sigma_c$  refers to the yield stress,  $G$  is the shear modulus,  $b$  is the length of the Burgers vector and  $M$  is Taylor's factor. Anelastic strain, as it is defined here, is related to the dislocations' subcritical bowing during loading below the yield stress (and mechanically reversible bowing during unloading), which are assumed to be time-independent at room temperature. Hence, the total true strain in the pre-yield regime ( $\epsilon_{pre}$ ) can be expressed as,

$$\epsilon_{pre} = \epsilon_a + \epsilon_e \quad (2)$$

where,  $\epsilon_e$  is the elastic true strain according to Hooke's law ( $\epsilon_e = \sigma/E$ ) with  $\sigma$  the applied stress and  $E$  the Young's modulus and,  $\epsilon_a$  the anelastic true-strain contribution because of dislocation movement [7,8]. Therefore, due to an extra strain component due to the occurrence of anelastic strain, the instantaneous slope ( $\theta_{pre}$ ) of the stress-strain graph in the pre-yield regime is not constant. It is lower than Young's modulus ( $E$ ), and decreases with increasing applied strain, where  $\sigma$  is the true stress:

$$\theta_{pre} = \left( \frac{d\sigma}{d\epsilon_{pre}} \right) < E \quad (3)$$

van Liempt and Sietsma [7] introduced a model that describes the stress-strain behaviour of a material in the pre-yield range based on fundamental concepts of dislocation theory. It considers the physical yield criterion of metal as the transition from reversible dislocation bowing to dislocation multiplication. The activation of Frank-Read sources is considered as the physical mechanism for dislocation multiplication, which forms the onset of plastic deformation in the physical yield criterion. This becomes apparent in an extended Kocks-Mecking plot, where the slope ( $\theta$ ), given by Eq. (3), is plotted as a function of the applied tensile stress ( $\sigma$ ). An expression for the strain is given as a function of the applied tensile stress, considering the bow-out area as indicated in Fig. 3. This expression upon differentiation and using the Taylor factor for converting shear stress to tensile stress gives  $\theta_{pre}$ , the pre-yield modulus as,

$$\theta_{pre} = \frac{M^2 E s^3 \sqrt{1-s^2}}{M^2 s^3 \sqrt{1-s^2} + \rho L^2 (1+\nu) (s - \arcsin(s) \sqrt{1-s^2})} \quad (4)$$

where,  $s = \sigma/\sigma_c = \sigma L/MGb$  is the normalised tensile stress,  $\nu$  is the Poisson's ratio and  $\rho$  is the dislocation density. The bowing out motion of dislocations occurs only for mobile dislocations, hence  $\rho$  refers to mobile dislocation density throughout this study. Eq. (4) shows that the pre-yield modulus is found to depend on the applied stress and the dislocation structure. Therefore, the pre-yield modulus is considered to characterise the non-linearity, as observed in stress-strain behaviour, and can be used to quantify the dislocation structure.

### 3. Results and discussion

#### 3.1. Quantification of dislocation structure at increasing plastic strain

A tensile test performed with incremental plastic deformation of 0.5% between each cycle for 5 cycles is shown in Fig. 4, which forms the basis for the application of the pre-yield model and thus characterisation of the dislocation structure in the material. The resulting graph reveals a broadening of hysteresis loops with each consecutive cycle, which will be discussed further in Section 3.2. In order to analyse the anelastic behaviour, the instantaneous slope of a true stress-true strain curve (i.e.,  $\theta = d\sigma/d\epsilon$ ) is plotted in Fig. 5,

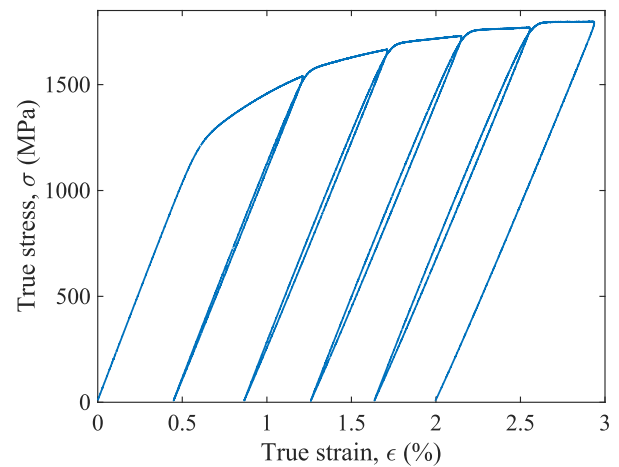


Fig. 4. A representative true stress-true strain curve for Stavax steel with 0.5% incremental plastic strain for five cycles.

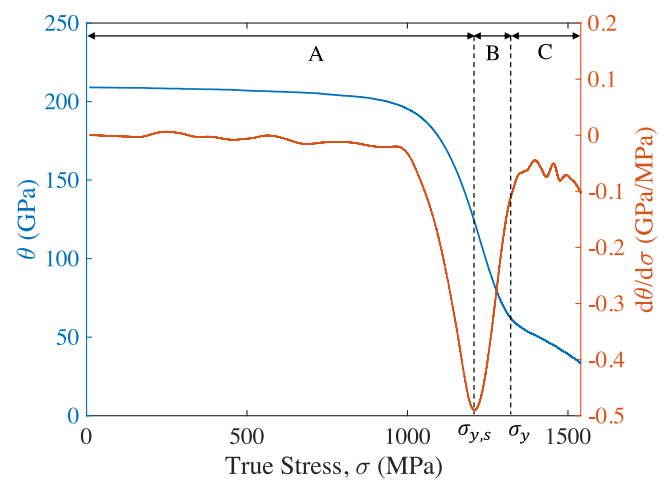
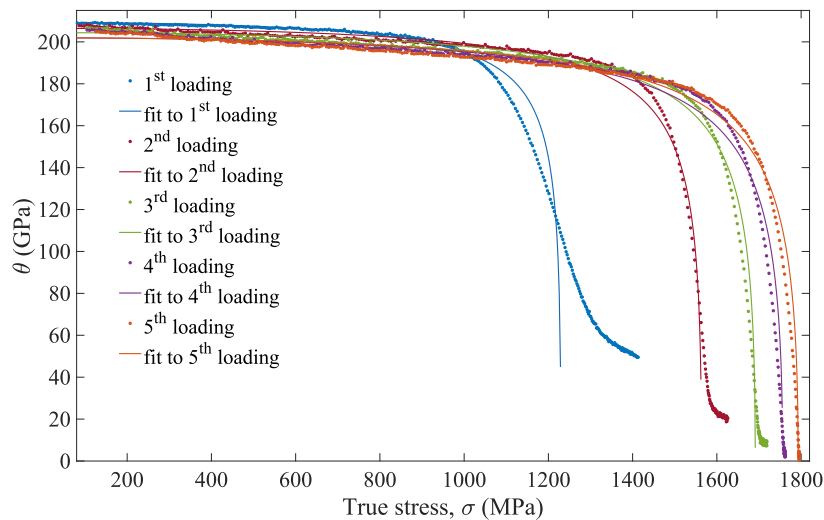


Fig. 5. Extended Kocks-Mecking plot (in blue) and a plot of slope of extended Kocks-Mecking plot versus stress (in orange) for the first cycle. The latter plot is divided into three regions A, B and C representing stages of pre-yielding and yielding.  $\sigma_{y,s}$  is the stress at which yielding begins to occur and  $\sigma_y$  is defined as the yield stress.

as a function of true stress, referred to as the extended Kocks-Mecking plot [7,29]. For the calculation of the pre-yield modulus for extended Kocks-Mecking plots, the true stress-true strain data has been smoothed using a robust locally weighted linear regression. The span for smoothing is chosen to be 10% of the total data points of around twelve thousand for each loading cycle, which results in a strain resolution of 0.0001% in the smoothed data. This limit is well within the acceptable strain resolution, which ensures a smooth curve without loss of accuracy. This smoothing procedure becomes necessary as the outliers or even small scatter in the raw data could otherwise lead to a large scatter upon calculating the differential for the slope.

#### 3.1.1. The extended Kocks-Mecking plot for a first loading situation

Fig. 5 shows the measured development of instantaneous slope ( $\theta$ ) as a function of the stress for the first loading cycle. At near zero stress level, a pre-yield modulus ( $\theta_{pre}$ ) of 210 GPa is found. At rising stress levels, the pre-yield modulus gradually decreases, obtaining a value of 200 GPa at reaching a stress level of 1000 MPa in the extended Kocks-Mecking plot. This gradual decrease of the pre-yield modulus right from the start is related to the anelastic strain, hypothesised to be associated with the progressing bowing out of dislocations, as discussed before. Above a stress level of 1000 MPa,



**Fig. 6.** Pre-yield model fitted to the extended Kocks-Mecking plot for all five loading curves up to  $\sigma_{y,s}$  (i.e., stress at the end of region A) for a representative sample. The fit gives the parameters for dislocation structure, namely dislocation segment length and dislocation density.

the pre-yield modulus decreases more rapidly as expected based on Eq. (4). A more moderate and transition to a linear hardening rate is observed at around 1300 MPa and above. This signals the onset of significant plastic deformation, also known as the stage III work hardening [29,30]. This transition, when distinctly present, is defined as the yield stress  $\sigma_y$  as described in [7]. However, this transition to yield stress from the pre-yield region is not sharp for the material used in this paper (it is indicated as region B in Fig. 5) and other materials [8].

Since a distribution of dislocation segment lengths is expected in the material, Frank-Read sources will be activated at a range of stress levels. Therefore, the wider the range of the segment lengths, the less sharp the transition. This effect of gradual variation in slope becomes more apparent in the slope of the pre-yield modulus, plotted against stress in Fig. 5. It is observed that at around 1200 MPa, a sharp drop in the slope of extended Kocks-Mecking plot reaches a minimum at  $\sigma_{y,s}$  after which the change in slope increases again. From this graph, we can hypothesise that the dislocation motion is no longer confined to bowing only;  $\sigma_{y,s}$  represents the start of the yield region (region B), which covers a certain stress range due to the distribution of dislocation segment lengths. The dislocation segments which are longer in length, yield or multiply at lower stresses than the shorter segments, giving rise to plasticity (Eq. (1)). For better understanding, the plot is divided into three regions. Region A refers to the stress until which the dislocation structure remains constant, the pre-yield region. It ends at the inflection point in  $\theta_{pre}$  as a function of  $\sigma$ , a phenomenon that is not reflected by Eq. (4). Region B is referred to as the range of stress where yielding initiates, and the dislocation structure starts to change. Region C refers to conventional plasticity or stage III work hardening. We define the stress at the transition A-B as the yield start  $\sigma_{y,s}$  and the transition B-C as the yield stress  $\sigma_y$ .

### 3.1.2. The effect of plasticity on extended Kocks-Mecking plots

In Fig. 6, the extended Kocks-Mecking plot for all five consecutive loading cycles for a representative sample is shown along with the applied pre-yield model fits. The extended Kocks-Mecking plot for the first cycle shows a more gradual transition to the yield stress  $\sigma_y$  than the consecutive cycles. The transition to yield stress becomes sharper, i.e., the width of region B decreases, with increasing plastic deformation as seen in Fig. 6. Furthermore, the slope change in the region A becomes steeper with increasing plastic deformation for consecutive cycles. This gradual transition

to yielding for martensite is consistent with the literature which shows a narrowing of X-ray line profiles with plastic deformation, unlike other metallic materials [25,31]. It has been attributed to internal strains developed during austenite shear transformation to martensite during quenching. Moreover, internal and residual stresses leading to strain inhomogeneity within the material has been attributed to anelastic strain contribution [6,10]. Further, the microstructural features described in Section 2.1 influence the dislocation structure, affecting the anelastic strain and the pre-yield modulus. The initial dislocation structure, which comprises a distribution of segment lengths pinned by microstructural features, changes upon plastic deformation in the first loading cycle. During the first loading cycle, the dislocation density increases through the Frank-Read mechanism and the interaction between dislocations becomes more intense. This causes the narrower distribution of segment lengths that is observed.

Additionally, Fig. 6 reveals that there is a decrease in the initial pre-yield modulus as the plastic deformation increases. This is in accordance with Schoeck's approximation [4] valid at low stresses, which states the pre-yield anelastic modulus is inversely proportional to the dislocation density, as well as with Eq. (4). Hence, with an increase in dislocation density due to plastic deformation, the initial value of the pre-yield modulus decreases. However, this decrease in the initial pre-yield modulus between the first and fifth loading cycle is only about 1% at stresses below 50 MPa. In literature, it has been noted that a depreciating trend in the E-modulus is generally found at plastic strains above 5% [32–36].

### 3.1.3. Applying the model

The pre-yield model allows the characterisation of the two parameters reflecting the dislocation structure in the specimen: dislocation density ( $\rho$ ) and average dislocation segment length ( $L$ ). The physics-based pre-yield model given by Eq. (4) is fitted to the extended Kocks-Mecking plots using the non-linear least-squares approach. Material parameters used are  $\nu = 0.3$ ,  $M = 3.06$ , and  $b = 0.248$  nm. As stated previously, the dislocation structure remains constant until the end of region A, i.e., until the minimum of the slope of the extended Kocks-Mecking plot. This is related to the derivative of pre-yield slope with respect to applied stress given by the pre-yield model (Eq. (4)) not showing a minimum. Hence, the pre-yield model is applied to the data until the stress reaches  $\sigma_{y,s}$  for each loading cycle, i.e., in region A.

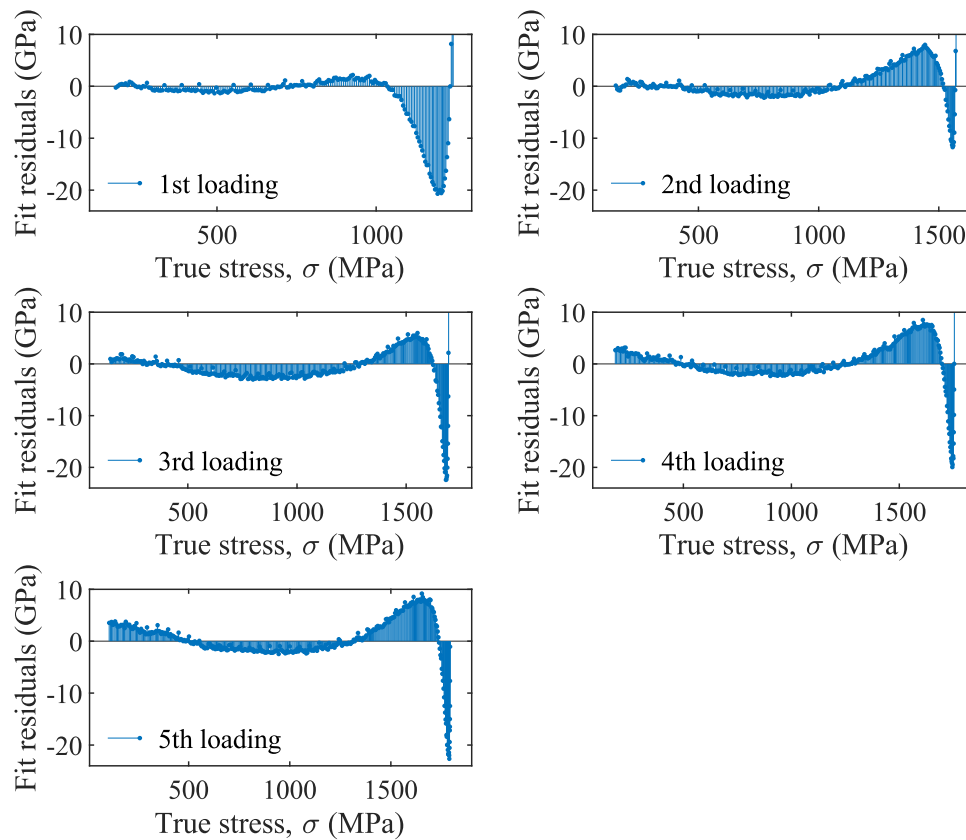


Fig. 7. Residuals of fit to the extended KM-plot (Fig. 6) show the goodness of fit with R-squared value of 0.99.

Table 3

Average dislocation density ( $\rho$ ) and effective segment length ( $L$ ), calculated through the pre-yield model.

Plastic strain (%)	$\rho$ ( $m^{-2}$ )		$L$ (nm)		$\rho L^2$		$\sigma_{y,s}$ (MPa)	
	Mean	SD	Mean	SD	Mean	SD	Mean	SD
0	$3.9 \cdot 10^{14}$	$0.2 \cdot 10^{14}$	52.1	0.11	1.05	0.60	1233	2
0.5	$8.2 \cdot 10^{14}$	$0.4 \cdot 10^{14}$	40.9	0.07	1.38	0.75	1569	3
1	$11.3 \cdot 10^{14}$	$0.3 \cdot 10^{14}$	37.9	0.03	1.62	0.55	1694	2
1.5	$14.0 \cdot 10^{14}$	$0.5 \cdot 10^{14}$	36.5	0.05	1.86	0.07	1758	2
2	$15.9 \cdot 10^{14}$	$0.3 \cdot 10^{14}$	35.8	0.02	2.04	0.45	1796	2

The pre-yield model's fit to the data reproduces the data excellently until at least up to 80% of the stress range for the first cycle and over 90% for the remaining cycles in region A. The residuals of the fit to the extended Kocks-Mecking plot show the goodness of fit with an R-squared value of 0.99 (Fig. 7). Despite a less accurate fit in the last part of region A, the trends in Fig. 6 are adequately followed by the model and the values of  $\rho$  and  $L$  (given in Table 3) are therefore representative of the dislocation structure even for a material with complex microstructure used in this study.

### 3.1.4. Dislocation structure characterisation

The range of yielding (region B) can provide an estimate of the range of dislocation segment lengths according to Eq. (1) (Fig. 8). This can serve as an approximation for the distribution range of segment lengths:  $L_{max} = MGb/\sigma_{y,s}$  and  $L_{min} = MGb/\sigma_y$ . This range narrows down as the dislocation density increases with increasing loading cycles. The average dislocation segment length,  $L$  obtained from a fit of the pre-yield model is within 0.2% to the maximum length of the segment length,  $L_{max}$ . This reflects the segment length distribution to be very narrow. The values of  $\rho$  and  $L$  calculated for all four cycles are summarised in Table 3, together with their standard deviations of average (SD). The standard deviation here captures variations because of both fitting of the model to

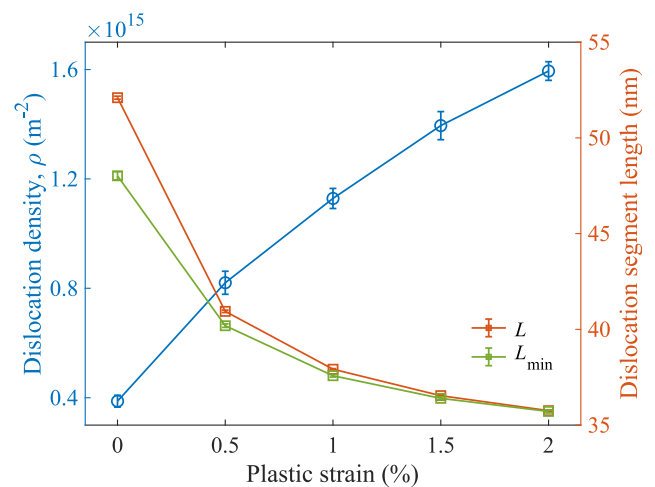
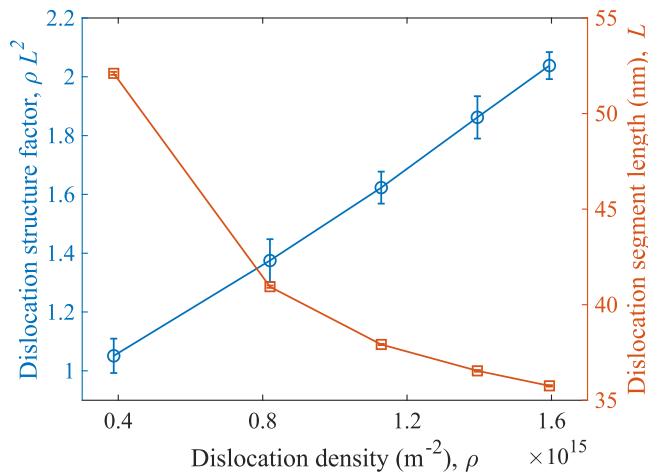


Fig. 8. Average dislocation density ( $\rho$ ) and dislocation segment length ( $L$ ) computed from the fit of pre-yield model to the data plotted as a function of the applied plastic strain for all samples.  $L_{min}$  is the average dislocation segment length at the yield stress  $\sigma_y$  (stress at end of region B in Fig. 5).



**Fig. 9.** Average dislocation structure factor ( $\rho L^2$ ) and average dislocation segment length ( $L$ ) variation as a function of the average dislocation density ( $\rho$ ) for all samples.

the data and the experimental error. As seen in Fig. 8, the dislocation density increases with increasing plastic deformation due to the multiplication of dislocations with increasing stress beyond the yield stress. And as more and more dislocations multiply and interact with each other because of the increasing dislocation density, the average dislocation segment length decreases with increasing plastic strain.

The dimensionless product  $\rho L^2$ , defined as the dislocation structure factor in this paper, represents the dislocation structure in terms of different combinations of dislocation density and average dislocation segment length. It is observed here that the denser the dislocation network (i.e., higher dislocation densities), the higher this product (Fig. 9). The  $\rho L^2$  value can be considered being an indicator of the dislocation network complexity [8,9]. The increase is in contrast to the usually considered Taylor's parameter,  $\alpha = (L\sqrt{\rho})^{-1}$ , which is considered being constant upon plastic deformation [9]. But, in some research, it has been shown that the coefficient  $\alpha$  in Taylor's model increases with increasing plastic deformation in martensitic steels, especially when the material undergoes a significant rearrangement of dislocation structure during deformation [37].

### 3.2. Hysteresis and unloading behaviour

Similar to the loading behaviour, unloading behaviour during the tensile test shows a clear departure from linearity, resulting in hysteresis occurring during the unloading and reloading (also seen in Fig. 4). This unloading behaviour has been related to dislocation pile-up and repulsion mechanism [14]. During unloading, the dislocation segments, piled up at the grain boundaries and other obstacles during loading, can move backwards, thus reducing the strain. Mobile dislocation segments can repel and move away from each other, while dislocation segments reduce the degree of bowing out as the external force reduces during unloading. The stress balance that results in Eq. (4) to describe the loading behaviour is lost during unloading. Dislocation rings emitted from Frank-Read sources will even lead to a strain increase while the stress is only slightly lowered. This is the onset of hysteresis. In addition, another reason for the hysteresis observed during unloading is due to the interaction of dislocations with obstacles in the microstructure [7]. The obstacles can be microstructural features, internal stresses and stresses from other dislocations such as the loops around a Frank-Read source. Such hysteresis in stress-strain curves has also been represented in recent literature due to internal stresses in the

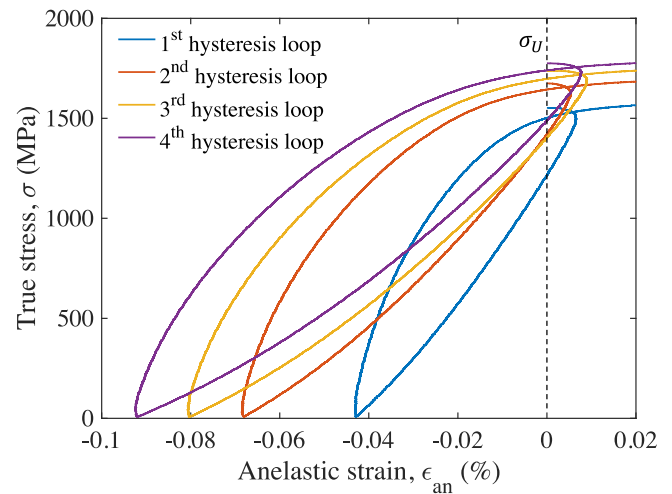


**Fig. 10.** True stress plotted against anelastic strain (given by Eq. (6)) shows the effect of anelastic strain on the hysteresis for all cycles. The dashed line in black indicates the stress at start of unloading  $\sigma_U$ , which is the zero point for anelastic strain in each cycle.

material due to strain inhomogeneity in the microstructure [6,38]. Internal stresses in the microstructure can also effectively act as obstacles, causing an additional stress on the dislocation segment hindering their movement. During loading, the obstacle presents an extra stress on the dislocation segment which changes in sign as the dislocation passes the obstacle. It continues to bow out further as the applied stress is further increased. During unloading, in the presence of an obstacle, the dislocation will be trapped behind the obstacle, unless the stress is reduced further for the dislocation to pass through the obstacle. This contributes to the hysteresis that is observed when loading-unloading below the yield stress. This dislocation movement results in a reduction in anelastic strain. This development of the anelastic component of the strain is seen to lead to a non-linear relationship between stress and strain during unloading. Increased deformation (or higher dislocation density in the material) before unloading results in greater deviations from linear unloading behaviour.

The unloading – reloading part of the curve is taken to start at the maximum stress, which is the point  $(\epsilon_U, \sigma_U)$  of the tensile curve. Here,  $\sigma_U$  is defined as the stress at which the applied load starts to decrease. At that point, the plastic strain  $\epsilon_p$  is given by:

$$\epsilon_p = \epsilon_U - \frac{\sigma_U}{E} \quad (5)$$

The dislocation structure has been influenced by the plastic deformation that has taken place up to this point and by the applied stress. The above equation defines the anelastic strain to be zero. Hence, in using Eq. (5), we set the reference value for the anelastic strain to be zero at  $\sigma_U$  to focus on the effect of anelastic strain exclusively during unloading and reloading. At any point  $(\epsilon, \sigma)$  of the unloading – reloading part, the anelastic strain  $\epsilon_{an}$  is given by:

$$\epsilon_{an} = \epsilon - \epsilon_p - \frac{\sigma}{E} \quad (6)$$

In order to better visualise the effect of anelastic strain on unloading behaviour, stress is plotted against anelastic strain  $\epsilon_{an}$  given by Eq. (6). A similar plot was introduced in recent literature by Li and Wagoner [6]. This enables a better scaling of the hysteresis loop, as seen in Fig. 10. At the starting point of unloading  $(\epsilon_U, \sigma_U)$  the anelastic strain is defined to be zero. At the lowest point during unloading, the dislocation structure is close to the equilibrium configuration. During unloading, it is important to note that initially the total strain increases by up to 0.002%, even though

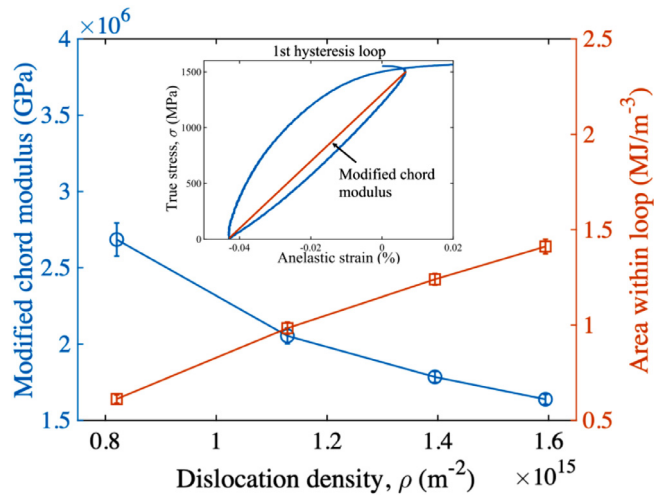


**Fig. 11.** Plot shows average modified chord modulus and area within hysteresis loops calculated for all samples. The inset figure shows the chord modulus calculation for the first unloading-reloading loop.

the applied load is reduced in a stress range of around 5 MPa. Similarly, the anelastic strain continues to increase with a decrease in the stress over a larger stress range of around 45 MPa as seen in Fig. 10. This increase in strain is attributed to the dislocation motion because dislocation loops around Frank-Read sources initially continue to expand at sufficiently high stresses. This follows from standard dislocation theory, since the radius of curvature of these loops is distinctly larger than the radius of curvature of the activated Frank-Read source, and as a consequence, the dislocation back-stress is relatively low.

Many phenomenological models have been proposed to partially or fully describe the nonlinear, path-dependent strain behaviour during unloading [14,15,39]. The most common approach is to define the effective elastic modulus as the slope of the straight line that relates the highest and lowest strain during unloading, named as chord modulus [34,39,40]. In this paper, a modified chord modulus approach is used. A modified chord modulus is given as the slope of the straight line that connects the point of maximum anelastic strain during unloading to the point of minimum stress during reloading (inset of Fig. 11). The modified chord modulus can be an order of magnitude higher (i.e., 2200 GPa), compared to the general chord modulus as the elastic strain is subtracted from the total strain in each cycle. The present approach also shows the asymmetry in the hysteresis loop between unloading and reloading curve with chord modulus as the secant. This experimental observation is in contrast with the usually assumed symmetry between loading-reloading curves [6,16,38]. The chord modulus defined in this way shows a decreasing trend with increasing dislocation density, as seen in Fig. 11, which indicates an increase in the anelastic strain effect. The energy loss due to hysteresis, in terms of the area within the hysteresis loop, is also seen to increase with increasing initial dislocation density at the beginning of each cycle.

### 3.3. Microplasticity: reversibility of anelastic strain

In tensile experiments, it is common to observe stress-strain hysteresis during loading-unloading cycles beyond the yield stress. However, older and recent research has shown that hysteresis occurs in the pre-yield region too due to anelasticity [7,8,20,41]. Due to the presence of obstacles such as solute atoms, precipitates, grain boundaries and other dislocations in the microstructure, the stresses on the dislocation to pass these obstacles is effectively re-

duced. This gives rise to hysteresis in the stress-strain curve. Depending on the dislocation structure in the material, closed stress-strain loops may not be obtained. As the dislocations present in the material have a range of segment lengths, some segments that are long will be activated as Frank-Read sources at low stress, even below  $\sigma_{y,s}$ . In addition, upon unloading, some dislocations may not get past the obstacles and thus not behave reversibly. These are contributing factors to the non-reversible strain that occurs, also known as microplasticity. Thus, unloading will not result in a closed stress-strain loop. Although this is contrary to the reported limit stress which close to the yield stress in recent research for several alloys below which no permanent plastic deformation is observed, closed loops were absent in the samples tested without an applied pre-strain similar to the case here [6].

A cyclic loading test was performed with four samples for 10 cycles each (Fig. 12 (a)). The maximum load in each cycle was 700 MPa, which is around 50% of the yield stress. Another test is performed on one sample up to the higher load of 900 MPa. Microplasticity or microplastic strain is defined as the strain at the end of each unloading cycle minus the strain at the end of the previous cycle [7,42]. A decreasing trend in the microplasticity with cycles can be seen in Fig. 12 (b). The microplastic strain at the end of the first loading cycle is observed to be considerably larger compared to the rest of the cycles. A similar occurrence has also been observed in recent research [7,8]. This difference in the microplastic strains at the end of the first unloading between the samples can have two reasons: macroscopic misalignment and microscopic dislocation behaviour. However, during testing, care was taken to minimise the misalignment in sample placement. Any possible misalignment that would occur is considerably small. An upward limit in misalignment of sample placement between the grips of  $2^\circ$  would result in a strain error of 15 microstrain [43], which is considered to be part of the random experimental error in the first cycle only. Note that the microplasticity in the first cycle is about 6 microstrain. To reduce this effect on the measurements, we consider the baseline for the calculation of the microplastic strain above the applied pre-load, at around 10 MPa.

The initial strain at 10 MPa during the first loading is subtracted from the total strain at the end of each loading-unloading cycle. This is because the strain at the low stress of 10 MPa during the first loading can safely be assumed to be elastic. Therefore, the subsequent strains give a clearer picture of effects of microplasticity strain contribution similar to the approach in Section 3.1.2. A plot of the total strain at the end of each loading-unloading cycle without the initial elastic strain from the first loading is plotted in Fig. 13. The total microplastic strain accumulates with increasing cycle number. Microplastic strain at stresses far below the yield stress indicates the occurrence of dislocation motion and role of obstacles in prohibiting dislocation motion. The plot shows an upward trend in total strain, with error bars (standard deviations of average values) for the samples loaded to 700 MPa indicating small variations between samples. It is worth noting that the strains here are quite small, of the order of  $10^{-3}\%$ . The increase in microplastic strain can be attributed to a similar phenomenon described in Section 3.2. Similar to the case of loading-unloading with plastic deformation, there is also a change in dislocation structure upon loading-unloading below the range of yielding. This change in dislocation structure is highest upon first unloading, as the structure becomes more “stabilised” with consecutive micro-plastic strains due to the dislocations with larger segments multiplying into smaller segment lengths. The interaction between dislocations becomes more restricted, and the dislocation structure stagnates after the first unloading cycle.

Overall, the quantification of dislocation density for scientific studies using the pre-yield model becomes more viable and scalable for the bulk of a material, as compared to the existing meth-

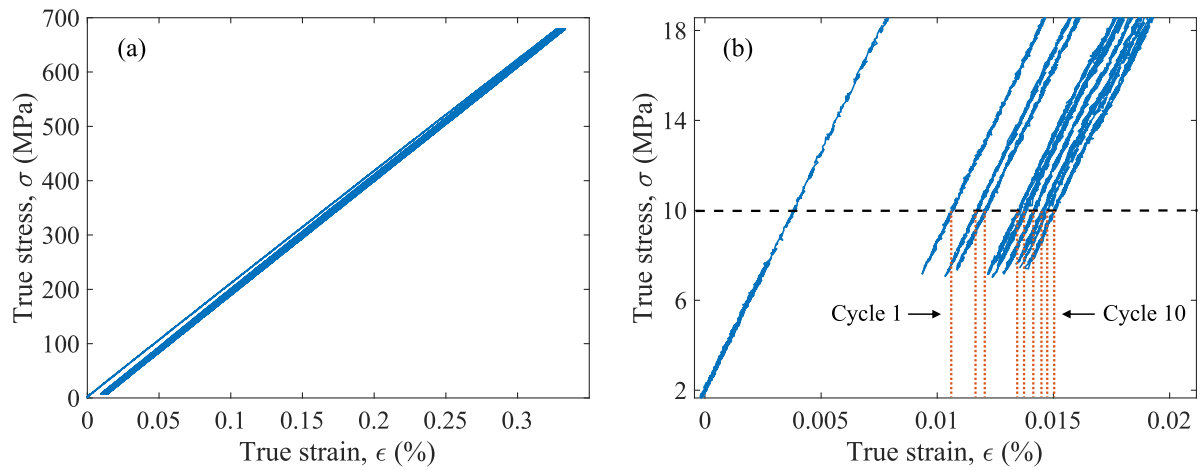


**Fig. 12.** (a) A representative true stress – true strain curve of cyclic testing below yield stress for 10 cycles and, (b) a detailed portion of the curve at stresses close to the pre-load showing the stress level (black dashed line) and the strains at the end of each cycle (orange dotted lines) used for calculation of microplastic strains.

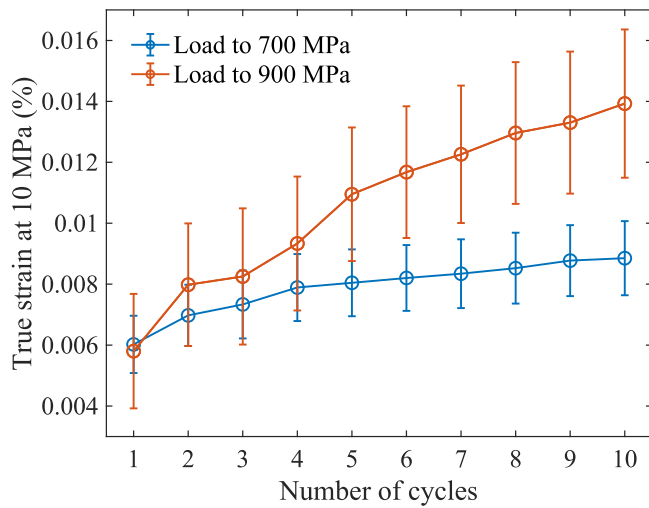


**Fig. 13.** Total strain at the end of each loading-unloading cycle (with strain zeroed at the initial strain during first loading) is plotted as a function of the cycle number for two sets of samples, one, loaded to 700 MPa and second, loaded to a higher stress of 900 MPa.

ods for quantification. Additionally, in applications that require high precision (in ranges of micrometre to sub-nanometre) and in the design and application of flexure components, this approach helps in gaining a better understanding of the non-linear elastic behaviour. The pre-yield model can be further developed to include the characteristics of microstructure such as grain boundaries, precipitate-dislocation interactions, dislocation character in different phases, and distribution of dislocation segment length.

#### 4. Conclusion

The main conclusions of the study are:

- In this study, the dislocation structure in terms of the dislocation density and segment length has been quantified by the application of a refined pre-yield model in martensitic stainless steel. With an R-squared value greater than 0.99 for all fits, it is shown for the first time that the pre-yield model can be applied to the quantification of dislocation structure even for complex microstructures and high strength steels, which validates the bowing model over a wide stress range. Insight into the start of yielding in the material is obtained based on ob-

- observations of the slope of extended Kocks-Mecking plot versus stress.
- The hysteresis and energy loss occurring during unloading-reloading with plastic deformation is related to the anelastic strain occurring due to mechanically reversible dislocation behaviour.
- Strain is not completely recovered upon loading-unloading at stresses well below the yield stress and microplasticity occurs owing to the underlying dislocation-bowing and dislocation-obstacle interaction mechanisms. The microplasticity occurring below yielding has been uniquely represented and quantified.

#### Declaration of Competing Interest

The authors declare that they have no known competing financial interests or personal relationships that could have appeared to influence the work reported in this paper.

#### Acknowledgements

This work is part of the research programme HTSM 2017 with project number 16210, which is partly financed by the Netherlands Organisation for Scientific Research (NWO) and co-financed by a consortium of partners that include Thermo Fischer, ASML, VDL ETG, Settels Savenije, DEMCON and 3D Systems. The authors would like to thank Krijn Bustraan from ASML for providing the material for this research. Dr. Timo Meinders of the University Twente is acknowledged for discussion on the initial increase of anelastic strain during unloading.

#### References

- [1] R.H.M. Schmidt, Ultra-precision engineering in lithographic exposure equipment for the semiconductor industry, *Philos. Trans. R. Soc. A Math. Phys. Eng. Sci.* 370 (2012) 3950–3972, doi:10.1098/rsta.2011.0054.
- [2] D.C. Handley, T.F. Lu, Y.K. Yong, C. Eales, Workspace investigation of a 3 DOF compliant micro-motion stage, in: *Proceedings of the 8th International Conference on Control, Automation, Robotics and Vision (ICARCV)*, 2, 2004, pp. 1279–1284, doi:10.1109/ICARCV.2004.1469030.
- [3] M. Ohring, *Mechanical behaviour of solids*, in: *Engineering Materials Science*, Academic Press, 1995, p. 299, doi:10.1016/B978-012524995-9/50031-3.
- [4] G. Schoeck, Dislocation theory of plasticity of metals, *Adv. Appl. Mech.* 4 (1956) 229–279, doi:10.1016/S0065-2156(08)70374-0.
- [5] G.J. van den Berg, The effect of the non-linear stress-strain behaviour of stainless steels on member capacity, *J. Constr. Steel Res.* 54 (2000) 135–160, doi:10.1016/S0143-974X(99)00053-X.
- [6] D. Li, R.H. Wagoner, The nature of yielding and anelasticity in metals, *Acta Mater.* 206 (2021) 116625, doi:10.1016/j.actamat.2021.116625.

- [7] P. van Liempt, J. Sietsma, A physically based yield criterion I. Determination of the yield stress based on analysis of pre-yield dislocation behaviour, *Mater. Sci. Eng. A* 662 (2016) 80–87, doi:10.1016/j.msea.2016.03.013.
- [8] Z. Arechabaleta, P. van Liempt, J. Sietsma, Quantification of dislocation structures from anelastic deformation behaviour, *Acta Mater.* 115 (2016) 314–323, doi:10.1016/j.actamat.2016.05.040.
- [9] Z. Arechabaleta, P. van Liempt, J. Sietsma, Unravelling dislocation networks in metals, *Mater. Sci. Eng. A* 710 (2018) 329–333, doi:10.1016/j.msea.2017.10.099.
- [10] Z. Chen, H.J. Bong, D. Li, R.H. Wagoner, The elastic–plastic transition of metals, *Int. J. Plast.* 83 (2016) 178–201, doi:10.1016/j.ijplas.2016.04.009.
- [11] R.M. Cleveland, A.K. Ghosh, Inelastic effects on springback in metals, *Int. J. Plast.* 18 (2002) 769–785, doi:10.1016/S0749-6419(01)00054-7.
- [12] Z. Chen, U. Gandhi, J. Lee, R.H. Wagoner, Variation and consistency of Young's modulus in steel, *J. Mater. Process. Technol.* 227 (2016) 227–243, doi:10.1016/j.jmatprotec.2015.08.024.
- [13] J. Mendiguren, F. Cortés, X. Gómez, L. Galdos, Elastic behaviour characterisation of TRIP 700 steel by means of loading-unloading tests, *Mater. Sci. Eng. A* 634 (2015) 147–152, doi:10.1016/j.msea.2015.03.050.
- [14] H. Kim, C. Kim, F. Barlat, E. Pavlina, M.G. Lee, Nonlinear elastic behaviors of low and high strength steels in unloading and reloading, *Mater. Sci. Eng. A* 562 (2013) 161–171, doi:10.1016/j.msea.2012.11.020.
- [15] L. Sun, R.H. Wagoner, Complex unloading behavior: nature of the deformation and its constitutive representation, *Int. J. Plast.* 27 (2011) 1126–1144, doi:10.1016/j.ijplas.2010.12.003.
- [16] A. Torkabadi, E.S. Perdahcioğlu, V.T. Meinders, A.H. van den Boogaard, On the nonlinear anelastic behavior of AHSS, *Int. J. Solids Struct.* 151 (2018) 2–8, doi:10.1016/j.ijsolstr.2017.03.009.
- [17] D. Hull, D.J. Bacon, *Introduction to Dislocations*, Butterworth-Heinemann, 2011.
- [18] M.M. Ashby, D.R.H. Jones, *Engineering Materials 1: An Introduction to Properties, Applications and Design*, Elsevier, 2012, doi:10.1016/C2009-0-64288-4.
- [19] C. Zener, J.H. Hollomon, Problems in non-elastic deformation of metals, *J. Appl. Phys.* 17 (1946) 69–82, doi:10.1063/1.1707696.
- [20] P.S. Alexopoulos, C.W. Cho, C.P. Hu, L. Che-Yu, Determination of the anelastic modulus for several metals, *Acta Metall.* 29 (1981) 569–577, doi:10.1016/0001-6160(81)90138-3.
- [21] R.K. Ham, The determination of dislocation densities in thin films, *Phil Mag* 6 (1961) 1183–1184, doi:10.1080/14786436108239679.
- [22] M.H. Loretto, *Electron Beam Analysis of Materials*, Springer, 1984, doi:10.1007/978-94-009-5540-0.
- [23] S. Morito, J. Nishikawa, T. Maki, Dislocation density within lath martensite in Fe-C and Fe-Ni alloys, *ISIJ Int.* 43 (2003) 1475–1477, doi:10.2355/isijinternational.43.1475.
- [24] T. Ungár, Microstructural parameters from X-ray diffraction peak broadening, *Scr. Mater.* 51 (2004) 777–781, doi:10.1016/j.scriptamat.2004.05.007.
- [25] B. Hutchinson, P. Bate, D. Lindell, A. Malik, M. Barnett, P. Lynch, Plastic yielding in lath martensites – an alternative viewpoint, *Acta Mater.* 152 (2018) 239–247, doi:10.1016/j.actamat.2018.04.039.
- [26] Uddeholm, Uddeholm Stavax ESR, (2013). <https://www.uddeholm.com/netherlands/nl/products/uddeholm-stavax-esr/> (accessed February 14, 2022).
- [27] ASTM E8 /E8M - 22, Standard Test Methods for Tension Testing of Metallic Materials, ASTM International (2022). doi:10.1520/E0008\_E0008M-22.
- [28] C. Frank, The Frank-Read source, *Proc. R. Soc. Lond. A Math. Phys. Sci.* 371 (1980) 136–138.
- [29] U.F. Kocks, H. Mecking, Physics and phenomenology of strain hardening: the FCC case, *Prog. Mater. Sci.* 48 (2003) 171–273, doi:10.1016/S0079-6425(02)00003-8.
- [30] A.D. Rollett, U.F. Kocks, A review of the stages of work hardening, *Solid State Phenom.* 35–36 (1993) 1–18, doi:10.4028/www.scientific.net/SSP.35-36.1.
- [31] B. Hutchinson, D. Lindell, M. Barnett, Yielding behaviour of martensite in steel, *ISIJ Int.* 55 (2015) 1114–1122, doi:10.2355/isijinternational.55.1114.
- [32] H.Y. Yu, Variation of elastic modulus during plastic deformation and its influence on springback, *Mater. Des.* 30 (2009) 846–850, doi:10.1016/j.matdes.2008.05.064.
- [33] H.Y. Yu, C.X. Zhou, Elastic modulus model based on dislocation density and its application on aluminum alloy 5052, *Key Eng. Mater.* 725 (2016) 659–664, doi:10.4028/www.scientific.net/kem.725.659.
- [34] F. Yoshida, T. Uemori, K. Fujiwara, Elastic-plastic behavior of steel sheets under in-plane cyclic tension-compression at large strain, *Int. J. Plast.* (2002) 633–659, doi:10.1016/S0749-6419(01)00049-3.
- [35] M. Yang, Y. Akiyama, T. Sasaki, Evaluation of change in material properties due to plastic deformation, *J. Mater. Process. Technol.* 151 (2004) 232–236, doi:10.1016/j.jmatprotec.2004.04.114.
- [36] J.A. Benito, J.M. Manero, J. Jorba, A. Roca, Change of Young's modulus of cold-deformed pure iron in a tensile test, *Metall. Mater. Trans. A Phys. Metall. Mater. Sci.* 36 (2005) 3317–3324, doi:10.1007/s11661-005-0006-6.
- [37] M. Shamsujjoha, Evolution of microstructures, dislocation density and arrangement during deformation of low carbon lath martensitic steels, *Mater. Sci. Eng. A* 776 (2020) 139039, doi:10.1016/j.msea.2020.139039.
- [38] G. Zhou, W. Jeong, E.R. Homer, D.T. Fullwood, M.G. Lee, J.H. Kim, H. Lim, H. Zbib, R.H. Wagoner, A predictive strain-gradient model with no undetermined constants or length scales, *J. Mech. Phys. Solids* 145 (2020) 104178, doi:10.1016/j.jmps.2020.104178.
- [39] F. Yoshida, T. Amaishi, Model for description of nonlinear unloading-reloading stress-strain response with special reference to plastic-strain dependent chord modulus, *Int. J. Plast.* 130 (2020) 102708, doi:10.1016/j.ijplas.2020.102708.
- [40] X. Xue, J. Liao, G. Vincze, A.B. Pereira, F. Barlat, Experimental assessment of nonlinear elastic behaviour of dual-phase steels and application to springback prediction, *Int. J. Mech. Sci.* 117 (2016) 1–15, doi:10.1016/j.ijmecsci.2016.08.003.
- [41] R. Maaß, P.M. Derlet, Micro-plasticity and recent insights from intermittent and small-scale plasticity, *Acta Mater.* 143 (2018) 338–363, doi:10.1016/j.actamat.2017.06.023.
- [42] N. Brown, K.F. Lukens, Microstrain in polycrystalline metals, *Acta Metall.* 9 (1961) 106–111, doi:10.1016/0001-6160(61)90053-0.
- [43] Z. Ma, H. Zhao, H. Cheng, J. Li, Effects of 2D misalignment on tensile results and corresponding correction methods to obtain the true stress-strain curve, *Meas. Sci. Technol.* 25 (2014), doi:10.1088/0957-0233/25/11/115011.